L. Kaffel Rebaï
Unité de Recherche en Mécanique et Energétique,
Ecole Nationale d'Ingénieurs de Tunis,
2000 Tunis,
Tunisia and IMFT,
UMR 5502 CNRS,
Université Paul Sabatier,
118 route de Narbonne,
31062 Toulouse,
France
e-mail: leila.kaffel@enit.rnu.tn

A. K. Mojtabi
IMFT, UMR 5502 CNRS,
Université Paul Sabatier,
118 route de Narbonne,
31062 Toulouse,
France

M. J. Safi
Unité de Recherche en Mécanique et Energétique,
Ecole Nationale d'Ingénieurs de Tunis,
2000 Tunis,
Tunisia

A. A. Mohamad
Department of Mechanical and Manufacturing Engineering,
The University of Calgary,
Calgary, AB, T2N 1N4,
Canada

A Linear Stability Study of the Gradient Zone of a Solar Pond

The linear stability of a plane layer with horizontal temperature and concentration stratification corresponding to gradient zone of a solar pond is investigated. The problem is described by Navier-Stokes equations with Boussinesq-Oberbeck approximation. Two source terms are introduced in the energy equations: the absorption of solar energy characterized by the extinction radiative coefficient μ_e and by the parameter f defined as the ratio of extracted heat flux to absorbed heat flux in the lower convective zone. The influence of the parameters μ_e and f on the onset of thermosolutal convection in the case of confined and infinite layers is analyzed. It is found that convection starts in an oscillatory state, independently of the $\mathrm{Ra_S}$ *value. Different convection solutions were found for marginal stability and steady state.* [DOI: 10.1115/1.2210498]

Keywords: solar pond, thermosolutal convection, linear stability, oscillatory state

1 Introduction

A solar pond is an artificial basin of water with a high concentration of salt at the bottom and a sufficiently uniform gradient, almost zero at the top. It is constituted by three well-defined zones (Fig. 1); the upper and lower convective zones (UCZ and LCZ, respectively), where temperature can be considered as uniform, flank the gradient zone (GZ) characterized by a concentration and temperature gradient. In fact, in this zone the salt gradient prevents convection and generates a temperature gradient as a result of solar energy absorption. Because of the poor heat conduction of water, the gradient zone plays a role of a transparent insulator and heat is trapped and stored in the lower zone, also called the storage zone.

The gradient zone is typically a double diffusive layer of salt and temperature and is subject to instabilities resulting from the difference in the rate of diffusion of salt and temperature. The main problem in a solar pond is thus the maintenance of the stability and the nonconvectivity of the gradient zone.

The majority of solar pond studies since the pioneering work of Wienberger [1], Tabor [2], and Rabl and Nielsen [3] have been experimental investigations. Based on experimental data of the steady-state condition, Hull et al. [4] suggested an empirical relation between the salinity and the temperature gradients in the nonconvective zone (NCZ).

In the 1980s, two models have been proposed to explain Nielsen's equilibrium condition. The *microconvection* model proposed by Hull and Mehta [5], which failed to predict the growth and the erosion rate of the gradient zone. The second model is the *thermal burst* model of Witte [6], based on the diffusive process at the interface. The interface shifting corresponds to the movement of the point of neutral buoyancy, which depends on the stability rate of the density. Later, Hull and Katti [7] proposed a modification of the microconvection model and predicted an equilibrium condition in agreement with the Nilesen's equilibrium correlation for a wide range of temperature gradients. Zangrando and Fernando [8] incorporated the effect of convection in the thermal burst model. Sreenivas et al. [9] later proposed a model that takes into account the effect of turbulent entrainment and diffusion on the growth/erosion of the NCZ. Their predictions indicate the dependence of the equilibrium condition on the height of the LCZ, apart from the salinity and temperature gradients of the NCZ. However, all the above-mentioned models were not adopted in linear stability analysis.

The first studies to consider the linear stability of an infinite layer with a linear vertical gradient of solute heated from below (by which GZ could be approximated to some extent) were developed in the 1960s [10–12]. These studies showed the existence of oscillatory motion leading to steady, convecting cellular motions with large heat flux. However, they considered constant diffusion coefficients in the layer and imposed values for the boundary conditions relative to the variables, which are rarely met in real solar ponds compromising the practical usefulness of such studies. Bemporad and Rubin [13] investigated the development of instabilities stemming from the multiselective injection and withdrawal procedures that create the stratified thermal layer of the advanced solar pond. They provide a realistic characterization of the extracted heat from a solar pond.

Recently, Giestas et al. [14,15] have performed a linear stability study of the gradient zone considered as a confined layer. They proposed a simplified mathematical treatment to model this zone

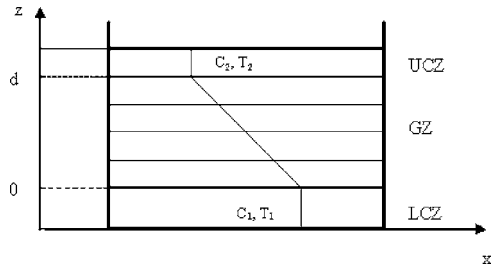

Fig. 1 General structure of a solar pond

and used a weak formulation of the governing equations and a Galerkin method expanded to the first order to obtain approximate solutions. They used trial functions similar to those used by Veronis [11] for a binary layer of infinite extension with free-free boundaries and constant temperature and concentration at top and bottom. They [15] also studied the contribution of nonconstant diffusion coefficients for the stability of the gradient layer together with the influence of solar radiation absorption.

In this work, we performed a linear stability study of the gradient zone using the mathematical formulation proposed by Giestas et al. [14]. However, the present study is not restricted to the first-order Galerkin approximation. The trial functions adopted in the present work satisfy boundary conditions. Calculations are conducted until convergence insured.

2 Mathematical Formulation

For isothermal flows, the two-dimensional (2D) perturbations are more destabilizing and therefore lead to the smallest values of critical Rayleigh number (Squire theorem). In the case of thermosolutal convection, this property was verified by Karimi-Fard et al. [16].

For the two-dimensional linear stability study, the gradient NCZ was modeled by a rectangular slab with free-free top and bottom surfaces, with constant concentrations C_1 and C_2 on both sides. We impose conduction heat flux at the bottom and convection flux at the top. The mathematical model can be described by Navier-Stokes equations with the Boussinesq-Oberbeck approximation, where a source term is introduced into the energy equations. This source term is due to absorption of solar energy and characterized by the extinction radiative coefficient μ_e, and the extracted heat flux from the lower convective zone is taken in to the consideration. The governing equations can be written as follows:

$$\nabla \cdot \mathbf{V} = 0$$

Table 1 Critical values of Ra_T and wave number as a function of Ra_S for different trial functions, with $f=0.5$, $\mu_e=0.8$, Pr=7, and Le=100.

	$N=3$ FB: sin-cos		$N=3$ FB: polynôme	
Ra_S	Ra_T^{crit}	k^{ex}	Ra_T^{crit}	k^{ex}
0	471	1.77	417	1.77
100	4963	0.79	4949	0.79
500	20,576	0.54	20,444	0.56
1000	39,105	0.50	38,744	0.51
5000	174,392	0.56	170,790	0.57
10,000	326,826	0.6	318,473	0.60
50,000	1,427,169	0.50	1,340,341	0.60

$$\rho_m\left[\frac{\partial V}{\partial t} + (\mathbf{V}\cdot\nabla)\mathbf{V}\right] = -\nabla P + \mu\Delta\mathbf{V} - \rho_m[1 - \alpha(T - T_1) + \beta(C - C_1)]g\mathbf{k}$$

$$\frac{\partial T}{\partial t} + (\mathbf{V}\cdot\nabla)T = \kappa\Delta T + \frac{\dot{q}}{\rho C_p}$$

$$\frac{\partial C}{\partial t} + (\mathbf{V}\cdot\nabla)C = D\Delta C \tag{1}$$

where $\dot{q}$ is the rate of energy generation per unit volume in the layer and T_1, C_1 are temperature and concentration of the reference state, respectively. The boundary conditions are given by the following equations:

$$C = C_1, \quad \frac{\partial T}{\partial z} = -\frac{q}{\lambda}, \quad w = 0, \quad \text{and} \quad \frac{\partial u}{\partial z} = 0 \quad \text{for} \quad z = 0 \ \ \forall x$$

$$C = C_2, \quad \frac{\partial T}{\partial z} = -\frac{h_d[T(d) - T_\infty]}{\lambda}, \quad w = 0, \quad \text{and}$$

$$\frac{\partial u}{\partial z} = 0 \quad \text{for} \quad z = d \ \ \forall x$$

$$\frac{\partial C}{\partial x} = \frac{\partial T}{\partial x} = 0 \quad \text{and} \quad \mathbf{V} = 0 \quad \text{for} \quad x = 0 \quad \text{and} \quad x = L \ \ \forall z \tag{2}$$

where d is the depth of NCZ, C_1 and C_2 are the concentrations in the lower and upper layers, T_∞ is the external temperature, $q(d)$ is the heat flux at the upper boundary ($z=d$), λ is the thermal con-

Table 2 Critical values, for the gradient zone of a solar pond of infinite extension, of Ra_T and wave number as a function of Ra_S for different truncation numbers N, with $\mu_e=0.8$, $f=0.5$, Pr =7 and Le=100.

	$N=2$		$N=3$		$N=5$		$N=6$	
Ra_S	Ra_T^{crit}	k^{ex}	Ra_T^{crit}	k^{ex}	Ra_T^{crit}	k^{ex}	Ra_T^{crit}	k^{ex}
0	422	1.76	417.176	1.768	417.111	1.768	417.111	1.768
1000	38,973	0.5	38,744	0.506	38,748.5	0.506	38,748.48	0.506
5000	178,437	0.41	170,790	0.57	170,676	0.588	170,676	0.588
6000	212,190	0.4	201,391	0.6	201,066	0.607	201,068	0.607
7000	245,696	0.4	231,380	0.6	230,744	0.62	230,750	0.62
8000	278,997	0.4	260,845	0.60	259,802	0.64	259,816	0.64
9000	312,132	0.4	289,857	0.61	288,313	0.65	288,340	0.65
10,000	345,127	0.4	318,473	0.61	316,339	0.66	316,384	0.66
20,000	670,278	0.3	590,108	0.62	578,832	0.7	578,296	0.7
30,000	990,766	0.3	846,924	0.61	820,204	0.72	821,810	0.71
40,000	1,308,853	0.3	1,096,053	0.6	1,050,232	0.72	1,053,425	0.71
50,000	1,625,478	0.3	1,340,341	0.6	1,271,797	0.7	1,277,003	0.7

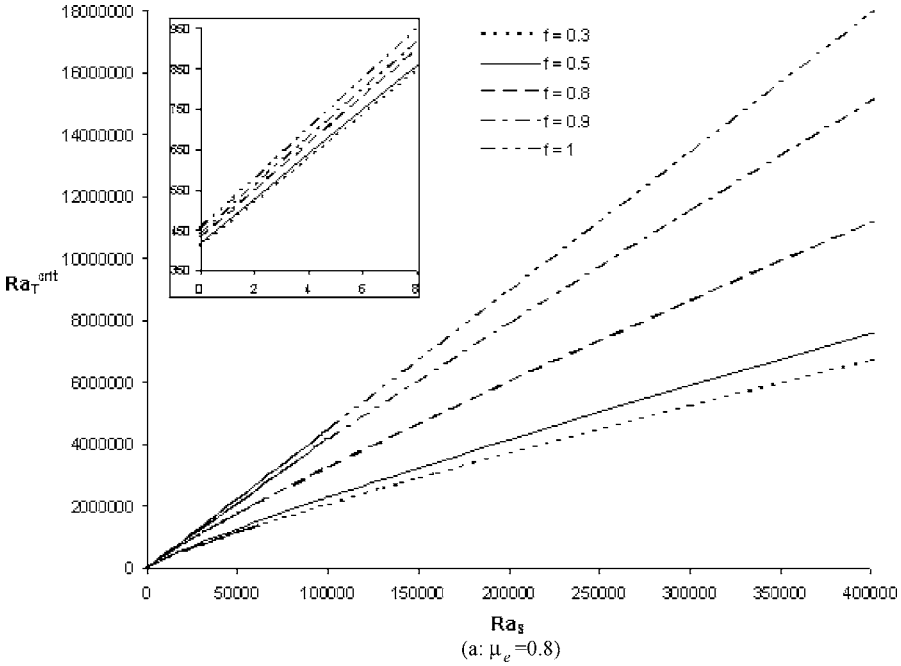

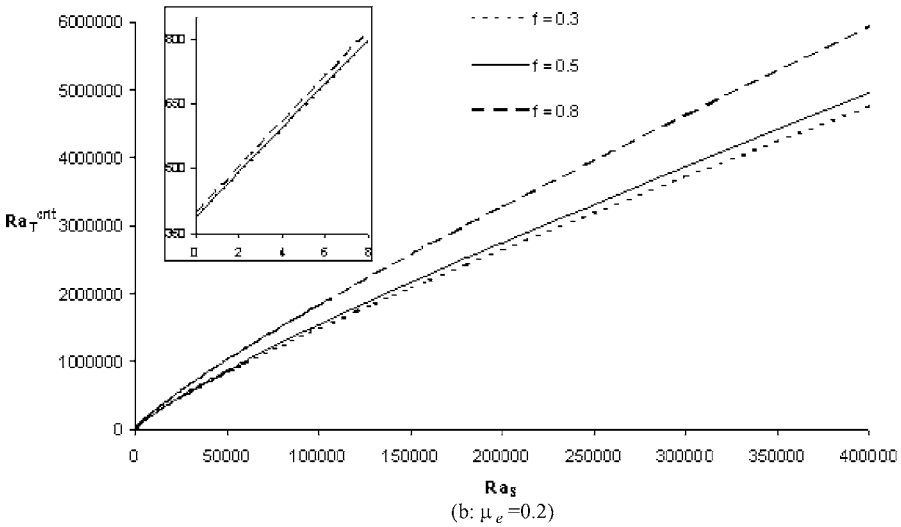

Fig. 2 Critical Rayleigh number as a function of solute Rayleigh number in the gradient zone of an infinite extension solar pond for different values of μ_e and f (Pr=7, Le=100, N=5): (*a*) μ_e=0.8 and (*b*) μ_e=0.2

ductivity of water, and h_d is the natural convection heat transfer coefficient.

2.1 Steady-State Solution of Temperature. The steady-state solution of temperature is obtained by equating to zero the velocity and all the partial derivatives with respect to time in the system of Eqs. (1). The equation for $T_S(z)$ reduces to

$$\frac{\partial^2 T_S}{\partial z^2} = -\frac{\dot{q}}{\lambda} \tag{3}$$

with

$$\frac{\partial T_S}{\partial z} = -\frac{q}{\lambda} \quad \text{for } z = 0 \ \ \forall x \quad \text{and}$$

$$\frac{\partial T_S}{\partial z} = -\frac{h_d[T_S(d) - T_\infty]}{\lambda} \quad \text{for} \quad z = d \ \forall x$$

The solar energy transmitted into the solar pond will be partially absorbed along its trajectory. The absorbed quantity depends on the wavelength, location, and concentration. For solar ponds of more than 1 m in depth, the major part of the solar spectrum is absorbed in the first five centimeters of the pond. Consequently, only short waves arrive to the bottom, are trapped, and increase the temperature of the water, reaching an average of 80°C. The absorption of solar radiation can be modeled by extinction coefficient μ_e, which takes into account the turbidity of the fluid (Lambert law). The rate of energy generation per unit volume is given by

$$\dot{q} = q(d)\mu_e e^{-\mu_e(d-z)} \tag{4}$$

where μ_e is the extinction coefficient.

Since the bottom of the pond is considered to be perfectly insulated, the heat flux from the storage zone (q) is equal to the

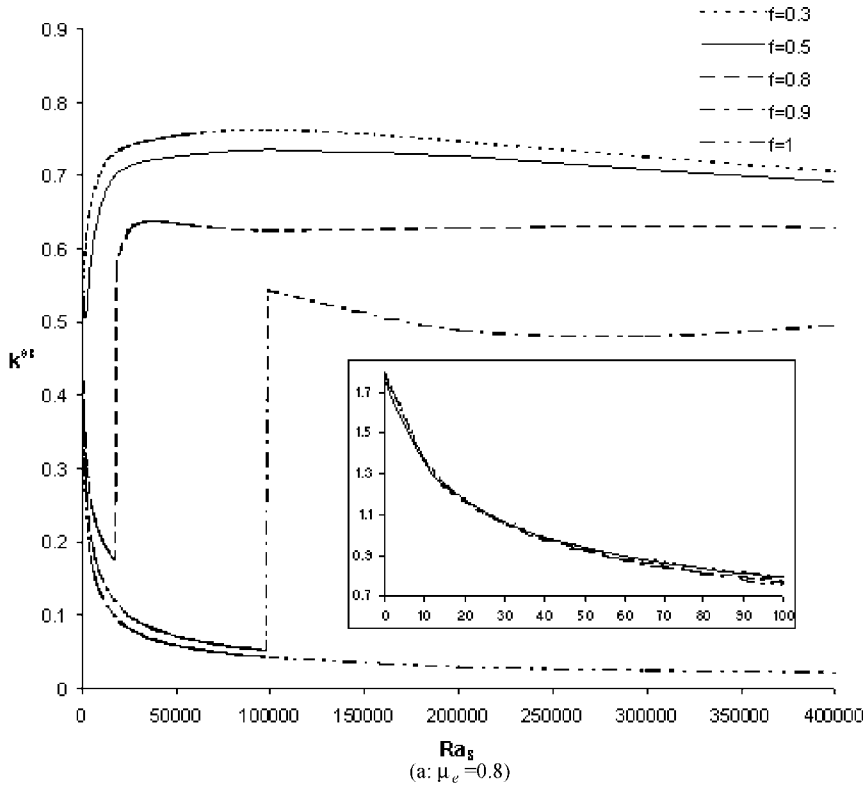

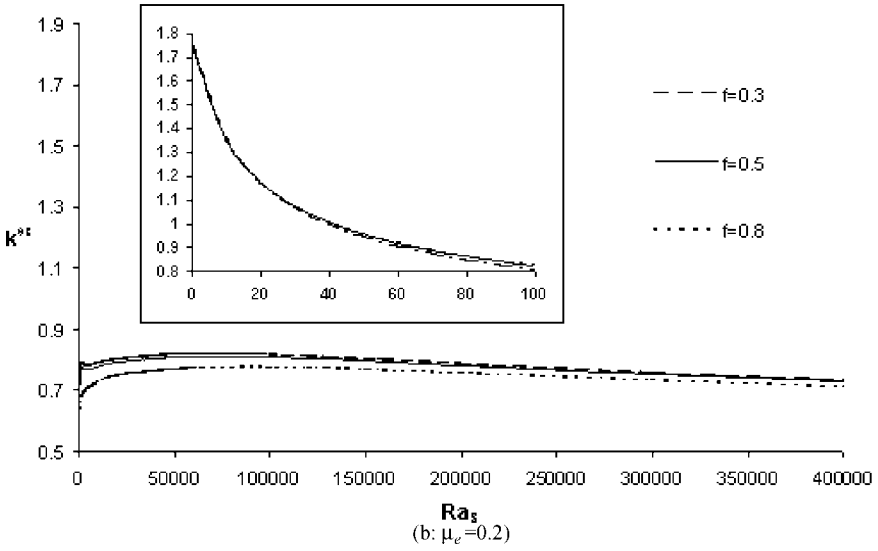

Fig. 3 Wave number as a function of solute Rayleigh number in the gradient zone of an infinite extension solar pond for different values of μ_e and f (Pr=7, Le=100, N=5): (*a*) μ_e=0.8 and (*b*) μ_e=0.2

difference between the total heat absorbed in the storage zone per unit area (q_{tot}) and the total heat extracted per unit area in the same zone (q_{ext})

$$q = q_{tot} - q_{ext} \tag{5}$$

It is assumed, for sake of simplification, that LCZ has an infinite height; thus,

$$q_{tot} = \int_{-\infty}^{0} \dot{q}(z)dz = q(d)e^{(-\mu_e d)} \tag{6}$$

The heat flux extracted (q_{ext}) is a fraction f of the total heat flux absorbed in LCZ $q_{tot}=fq_{abs}$ yielding

$$q = q_{tot} - q_{ext} = (1-f)q_{tot} = (1-f)q(d)e^{(-\mu_e d)} \tag{7}$$

The balance of heat flux through the gradient zone in the steady state is expressed as

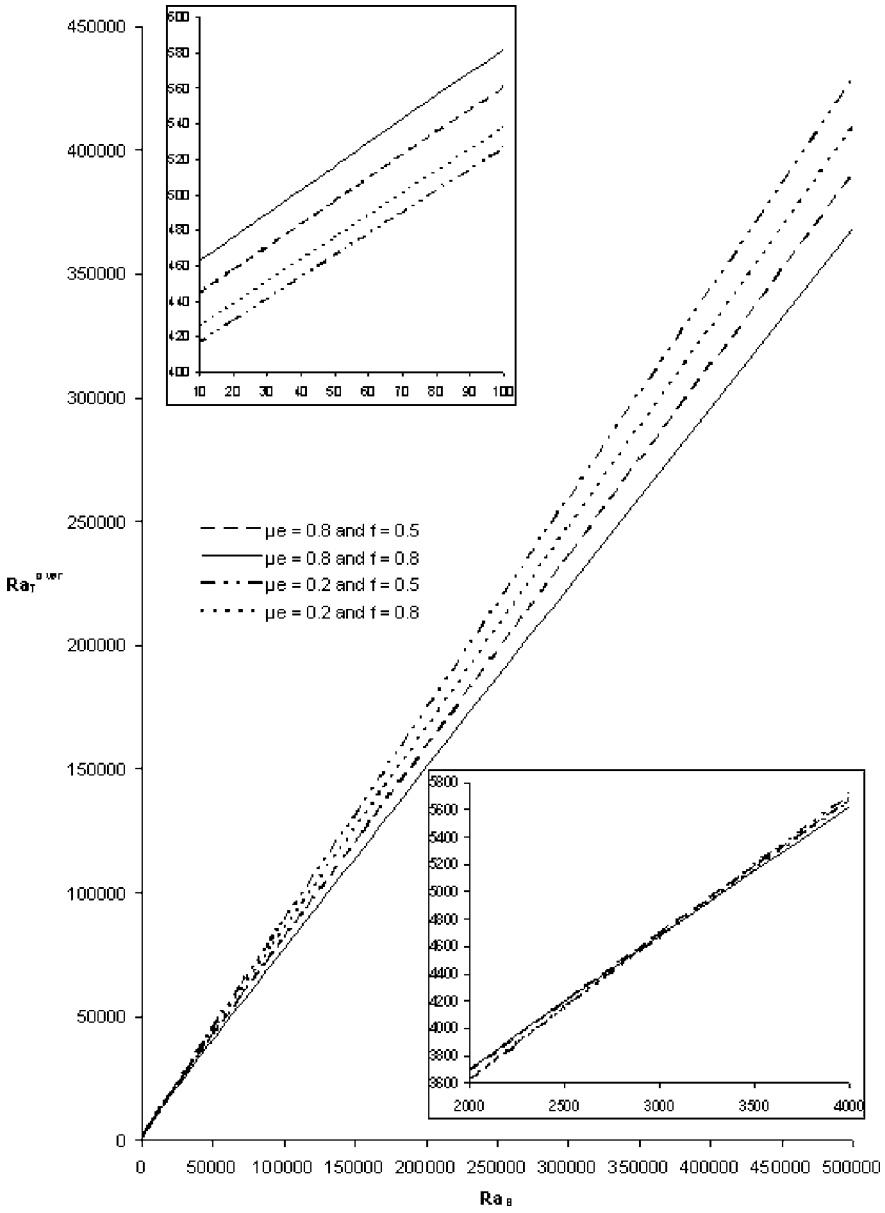

Fig. 4 Critical Rayleigh number of oscillatory state as a function of solutal Rayleigh number in the gradient zone of an infinite extension solar pond for different values of μ_e and f (Pr=7, Le=100, N=M=2)

$$q + \int_0^d q(d)\mu_e e^{(-\mu_e d)} e^{(\mu_e z)} dz = h_d[T(d) - T_\infty] \tag{8}$$

yielding:

$$q(d)[1 - fe^{(-\mu_e d)}] = h_d[T(d) - T_\infty] \tag{9}$$

From Equations (3), (4), (7), and (9), we get the steady-state solution for temperature

$$T_S(z) = T_\infty + \frac{q(d)}{\lambda} e^{(-\mu_e d)}\left[-\frac{e^{\mu_e z}}{\mu_e} + f(z-d)\right] - \frac{f}{h_d} q(d) e^{(-\mu_e)} + q(d) \times \left(\frac{1}{h_d} + \frac{1}{\lambda \mu_e}\right) \tag{10}$$

2.2 Steady-State Solution. The linear stability study concerned the following steady solution (base solution), where the stream function (it is introduced instead of the velocity), concentration, and temperature (Ψ_S, C_S, T_S), are given by

$$\Psi_S = 0$$

$$C_S(z) = \frac{C_2 - C_1}{d} z + C_1$$

$$T_S(z) = T_\infty + \frac{q(d)}{\lambda} e^{(-\mu_e d)}\left[\frac{e^{(-\mu_e z)}}{\mu_e} + (z-d)f\right] - \frac{f}{h_d} q(d) e^{(-\mu_e)} + q(d) \times \left(\frac{1}{h_d} + \frac{1}{\lambda \mu_e}\right) \tag{11}$$

Table 3 Critical values, for the gradient zone of a finite extension solar pond, of Ra_T and Hopf frequency as a function of Ra_S for different truncation numbers N and M with $A=1$, $Pr=7$, $Le=100$, $\mu_e=0.8$, and $f=0.5$.

	Steady state				Oscillatory state			
	$N=M=2$	$N=M=3$	$N=M=4$	$N=4,\ M=5$	$N=M=2$		$N=M=3$	
Ra_S	Ra_T^{crit}	Ra_T^{crit}	Ra_T^{crit}	Ra_T^{crit}	Ra_T^{over}	ω	Ra_T^{over}	ω
0	1426	1399	1337	1336	1424	0	1400	0
1000	82,301	90,715	90,856	90,433	2608	12.53	2564	12.54
5000	403,000	338,778	325,543	321,051	6621	30.36	6560	30.22
6000	484,100	400,198	382,721	375,346	7547	33.50	7491	33.35
7000	563,400	461,361	439,282	428,459	8460	36.37	8410	36.2
8000	642,600	522,347	495,338	480,559	9364	39.02	9319	38.85
9000	718,400	583,208	550,968	531,778	10,261	41.47	10,222	41.29
10,000	800,300	643,977	606,231	582,225	11,152	43.77	11,120	43.58
20.000	1,586,000	1,249,451	1,145,905	1,058,675	19,872	61.39	19,896	61.1
30,000	2,396,000	1,853,623	1,673,224	1,506,792	28,381	73.99	28,401	73.38
40,000	3,146,000	2,457,444	2,195,156	1,940,535	36,754	84.22	36,681	83
50,000	3,949,000	3,061,120	2,714,360	2,365,590	45,035	93.09	44,768	91.4

3 Linear Stability Analysis

In this study, two cases are considered, the first is an infinite extension layer and the second is a confined layer with rigid and thermally insulated lateral boundaries. The dependence of Ra_T^{crit} and exchange wave number (k^{ex}) on f for fixed μ_e and for different Ra_S values is subsequently described.

The perturbations imposed on the stream function, temperature, and concentration are denoted (ψ,θ,c), respectively. (Ψ,T,C) are hereafter expressed as

$$(\Psi,T,C)(x,z,t)=(\psi,\theta,c)(x,z,t)+(\Psi_S,T_S,C_S)(z) \tag{12}$$

The following reference parameters were used in order to express the linearized equations in a dimensionless form: ΔT for the temperature with $\Delta T=T_1-T_2$, ΔC for the concentration with $\Delta C=C_1-C_2$, κ for the stream function, d for length, d^2/κ for time, $\lambda\Delta T/d$ for the heat flux, and λ/d for the natural convection heat transfer coefficient. The set of dimensionless linear stability equations obtained are

$$\frac{\partial\Delta\psi}{\partial t}=\mathrm{Pr}\Delta^2\psi+\mathrm{Pr}\left(\mathrm{Ra}_T\frac{\partial\theta}{\partial x}-\mathrm{Ra}_S\frac{\partial c}{\partial x}\right)$$

$$\frac{\partial\theta}{\partial t}+\frac{\partial\psi}{\partial x}q(d)e^{(-\mu_e)}(e^{\mu_e z}-f)=\Delta\theta$$

$$\frac{\partial c}{\partial t}+\frac{\partial\psi}{\partial x}=\frac{1}{\mathrm{Le}}\Delta c \tag{13}$$

where $\mathrm{Pr}=\nu/\kappa$ and $\mathrm{Le}=D/\kappa$, with the following boundary conditions in confined layer:

$$\frac{\partial^2\psi}{\partial z^2}=\psi=c=0 \quad \text{for} \quad z=0 \quad \text{and} \quad z=1 \ \ \forall x$$

$$\frac{\partial\theta}{\partial z}=0 \quad \text{for} \quad z=0 \quad \text{and} \quad \frac{\partial\theta}{\partial z}-h_d\theta=0 \quad \text{for} \quad z=1 \ \ \forall x$$

$$\frac{\partial\psi}{\partial x}=\psi=\frac{\partial c}{\partial x}=\frac{\partial\theta}{\partial x}=0 \quad \text{for} \quad x=0 \quad \text{and} \quad x=A \ \ \forall z \tag{14}$$

where $\mathrm{Ra}_T=g\alpha\Delta TH^3/\kappa\infty$ and $\mathrm{Ra}_S=g\beta\Delta CH^3/\kappa\infty$ are the thermal Rayleigh number and the salinity Rayleigh number, respectively. Pr is the Prandtl number, Le is the Lewis number, and A is the aspect ratio. For an infinite extension layer, the same boundary conditions are used except the last condition for $x=0$ and $x=A$.

For a confined layer, the solutions of system (13) associated to the boundary conditions (14) are chosen as follows:

$$(\psi,\theta,c)(x,z,t)=[\psi(x,z),\theta(x,z),c(x,z)]e^{(\sigma t)} \tag{15}$$

where σ is a complex, $[\psi(x,z),\theta(x,z),c(x,z)]$ are functions of x and z variables. In the case of an infinite extension layer in the x direction, the stream function, temperature, and concentration are expanded in normal modes, and we get

$$[\psi(x,z),\theta(x,z),c(x,z)]=[\psi(z),\theta(z),c(z)]e^{(ikx)}e^{(\sigma t)} \tag{16}$$

where k is the wave number in the x direction, σ is a complex, and $i^2=-1$.

The weighted-residuals Galerkin method was used with polynomial trial functions verifying all the boundary conditions of the problem (14). The polynomial trial functions used for the case of confined layer are given as follows:

$$\psi(x,z)=\left(-\frac{x}{A}\right)^2\left\{\sum_{i=1}^{N}x^{i+1}[a_{i1}(z-2z^2+z^4)+a_{i2}(z+2z^3-6z^4+3z^5)]+\sum_{i=1}^{N}\sum_{j=3}^{M}a_{ij}x^{i+1}z^j(1-z^3)\right\}$$

$$\theta(x,z)=b_{01}[h_d(z^2-1)-2]+\sum_{j=2}^{j=M}b_{0j}z^j[(h_d+j)(z+1)+1]+\left[1-\left(\frac{i+1}{i+2}\right)\frac{x}{A}\right]+\left(\sum_{i=1}^{N}x^{i+1}\{b_{i1}[h_d(z^2-1)-2]+\sum_{i=1}^{N-1}\sum_{j=2}^{M}b_{ij}x^{i+1}z^j[(h_d+j)(z+1)+1]\}\right)$$

$$c(x,z)=(1-z)\left\{\sum_{j=1}^{M}c_{0j}z^i+\sum_{i=1}^{N-1}\sum_{j=1}^{M}c_{ij}x^{i+1}\left[1-\left(\frac{i+1}{i+2}\right)\frac{x}{A}\right]z^j\right\} \tag{17}$$

The adopted trial functions satisfy all the boundary conditions (14) and form a complete space function for the problem (13). In the case of an infinite extension layer, the following functions were used:

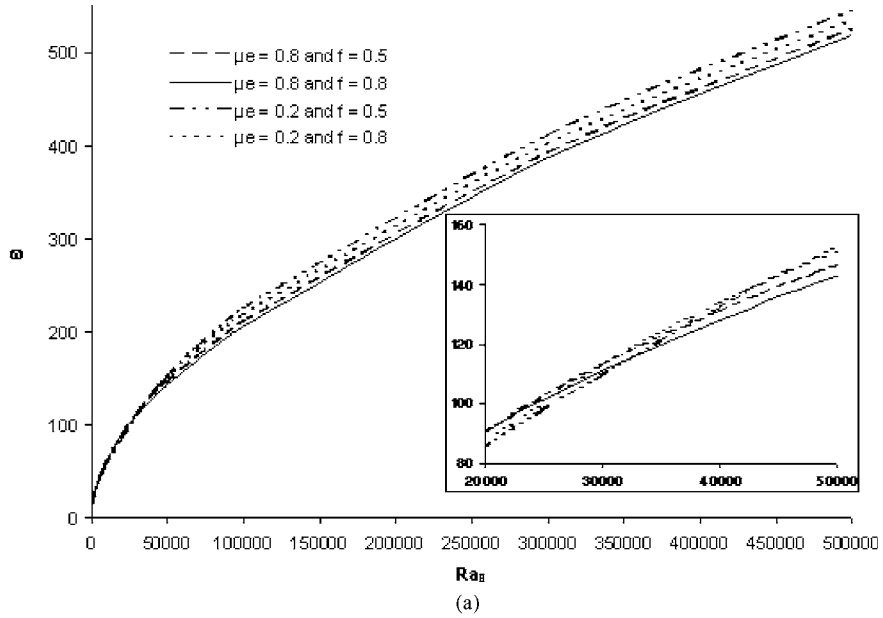

Fig. 5 Hopf frequency and wave number as functions of solutal Rayleigh number in the gradient zone of an infinite extension of a solar pond for different values of μ_e and f (Pr=7, Le=100, N=M=2): (*a*) Hopf frequency and (*b*) wave number as a function of solutal Rayleigh number

$$\psi(z) = a_1(z - 2z^3 + z^4) + a_2(z + 2z^3 - 6z^4 + 3z^5) + \sum_{i=3}^{N} a_i(1 - z)^3 z^i$$

$$\theta(z) = b_1(h_d z^2 - 2 - h_d) + \sum_{i=2}^{N} b_i z_i[h_d + 1 + i - (h_d + i)z]$$

$$c(z) = \sum_{i=1}^{N} c_i(1 - z)z^i \qquad (18)$$

4 Results and Discussion

The cases of infinite extension layer and confined layer are analyzed. In order to compare the present model results to those obtained by [14], the same values of physical parameters are used

$$\begin{cases} A = 1, \quad d = 1 \text{ m}, \quad \lambda = 0.6 \text{ w/m/}^\circ\text{C}, \quad h_d = 100 \text{ w m}^2/^\circ\text{C} \\ q(d) = 50 \text{ w/m}^2 \quad \text{for} \quad \mu_e = 0.2 \text{ m}^{-1} \\ q(d) = 66 \text{ w/m}^2 \quad \text{for} \quad \mu_e = 0.8 \text{ m}^{-1} \\ \text{Pr} = 7, \quad \text{Le} = 100 \quad \text{and} \quad f \text{ varying } 0.5 \text{ and } 1 \end{cases}$$

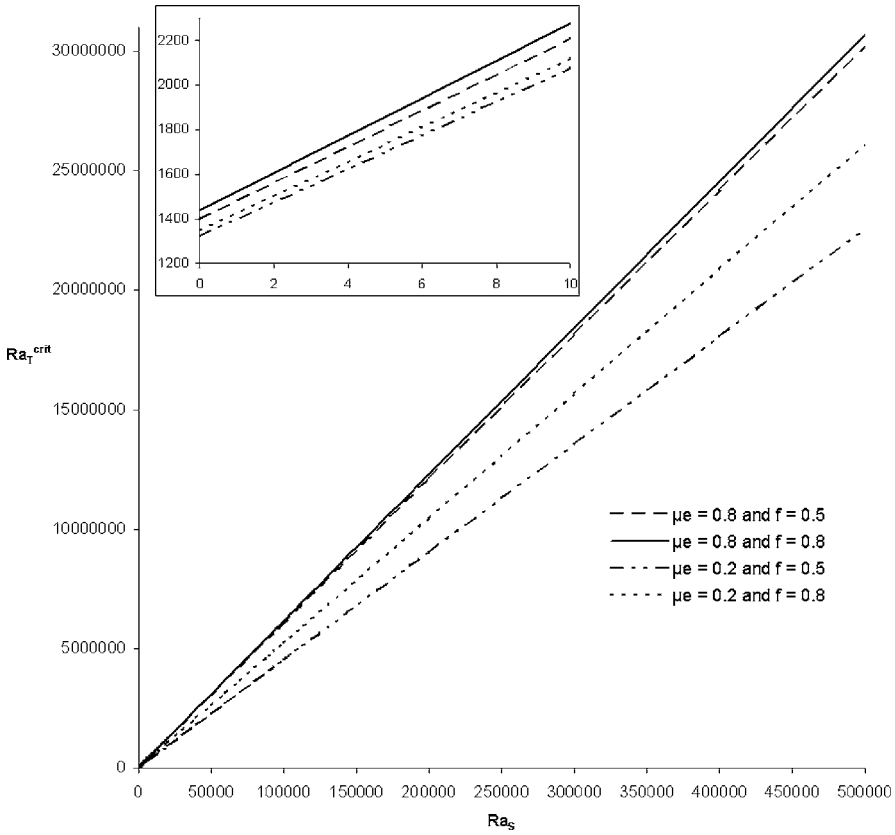

Fig. 6 Critical Rayleigh number of the steady state as a function of solutal Rayleigh number in the gradient zone of a finite extension solar pond for different values of μ_e and f (A=1, Pr=7, Le=100, N=2, M=3).

4.1 Infinite Extension Layer. First, two sets of trial functions were assayed in order to find the most appropriate one for our problem design; the first set is of the Fourier series type, in combination with the Tau method [17] and the second is of the polynomial type, where all trial functions verify all the boundary conditions. For the Fourier- (19) and polynomial- (18) type trial functions $[\psi(z), \theta(z), c(z)]$

$$\psi(z) = \sum_{i=1}^{N} a_i \sin(i\pi z), \quad c(z) = \sum_{i=1}^{N} b_i \sin(i\pi z), \quad \text{and} \quad (19)$$

$$\theta(z) = \sum_{i=1}^{N-1} c_i \cos\left(i\frac{\pi}{2}z\right)$$

Tables 1 and 2 show that convergence is faster when polynomial-type trial functions are used. Moreover, these functions are more representative of the problem studied as they satisfy only the boundary conditions of that particular problem. For these reasons, polynomial functions were subsequently chosen in this study.

In order to determine the effect of the truncation number N on the convergence of the trial functions, N was varied from 2 to 6, while fixing the parameters σ and μ_e. For the steady-state case, σ is set to 0, the extinction coefficient, μ_e is set to 0.8, the Prandtl number Pr is set to 7, the Lewis number Le is set to 100, and f is set to 0.5 (Table 2). It is seen that for small values of Ra_S, critical values of Ra_T and the wave number reach a plateau and remain almost constant after N=4. A small variation is, however, observed for large Ra_S values. Very small differences are observed between values found at the fifth and sixth orders; for example, the relative difference is only 0.41% for Ra_S=50,000. In Secs. 4.1.1 and 4.1.2 all computations were done at the order N=5.

4.1.1 Change of Stability (σ=0). Variation of the stationary critical Rayleigh number for temperature Ra_T^{crit} as a function of Ra_S (Fig. 2) shows that convection starts later for larger values of f; the system is more stable when more heat flux is extracted from the LCZ. The extinction coefficient has a stabilizing effect; the less the fluid is transparent, the more it is stable.

Variation of k^{ex} as a function of Ra_S (Fig. 3) shows that, for μ_e=0.2, the same behavior is found regardless of the f value (0.3, 0.5, and 0.8); for small Ra_S, the wave number k^{ex} decreases. When increasing Ra_S, k^{ex} increases and then decreases. For $f<0.8$, the same behavior was observed for μ_e=0.8 than for μ_e=0.2 (Fig. 3). For $f \geqslant 0.8$, increasing Ra_S, an important jump in the values of the wave number is observed. The jump is delayed (occurs at larger Ra_S values) as f increases and it disappears for f=1.0. This behavior could be explained by the fact that, for $f \geqslant 0.8$, there are two minima in the plan (Ra_T, k^{ex}). When increasing Ra_S, we note that the value of Ra_T at the first minimum increases, whereas the Ra_T value at the second minimum decreases until it goes below that of the first minimum. For f=1.0, no jump is observed even for Ra_S values as large as 1,000,000. The wave number tends to zero ($k \rightarrow 0$) when Ra_S increases; this means that for large values of Ra_S, the convective field is made up of a single convective cell.

4.1.2 Marginal Stability. The study of the linear marginal stability ($\sigma = \omega i$) of the gradient zone of a solar pond with infinite extension is presented. Convection occurs in the oscillatory state in a solar pond. In fact, Figs. 2 and 4 show that critical values of

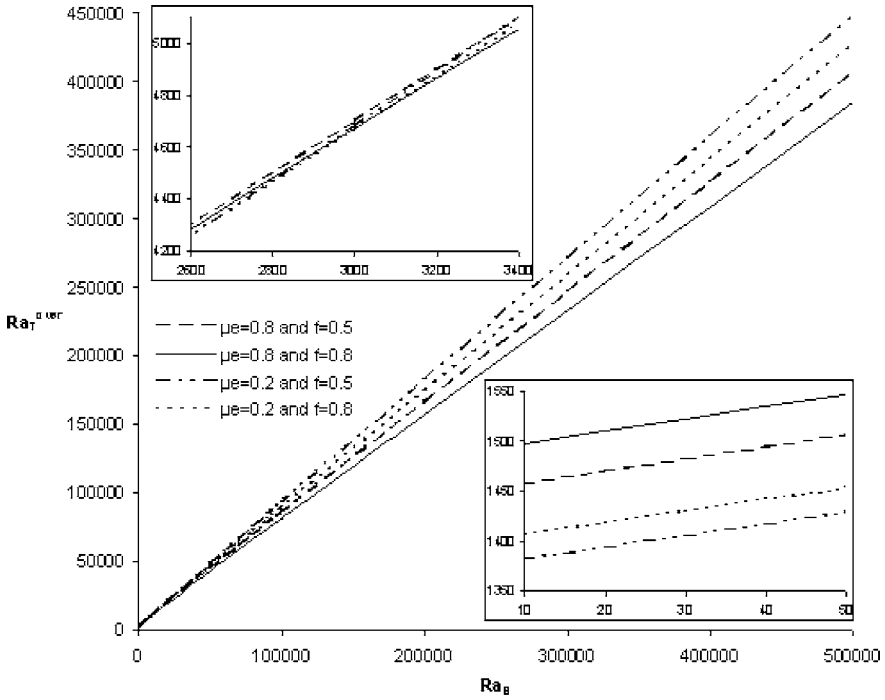

(a)

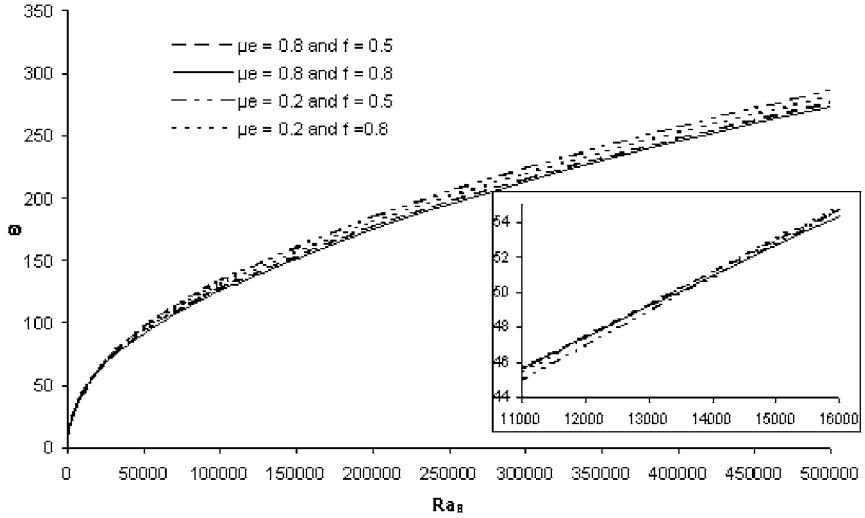

(b)

Fig. 7 Critical Rayleigh number and the Hopf frequency of the oscillatory state as functions of solutal Rayleigh number in the gradient zone of a finite extension solar pond for different values of μ_e and f (Pr=7, Le=100, N=M=2): (*a*) critical Rayleigh number and (*b*) Hopf frequency

Ra_T^{over} for the oscillatory state are smaller than those of the steady state, regardless of the solution transparency and the heat flux extracted in the storage zone. For large values of Ra_S, the ratio of critical Ra_T in the oscillatory and steady states, Ra_T^{over}/Ra_T^{crit} converges to 0.01. This finding is consistent with results of Veronis [10].

In the oscillatory state, variation of critical Ra_T (Ra_T^{over}) as a function of truncation number N, shows that Eqs. (1.3.4) converges rapidly to the *good* solutions starting from $N=3$ (Table 3). Evolution of Ra_T as a function of Ra_S (Fig. 4), shows that for $Ra_S \leqslant 1000$, convection has the same behavior than that in the steady state. As could be seen in Fig. 4, convection is delayed for less transparent solutions and when more heat flux is extracted in the storage zone (f increases). Above this Ra_S value, a different behavior is observed and convection is only slightly advanced when μ_e and f increase.

The same behavior in the evolution of Hopf frequency and wave number k^{ex} as a function of Ra_S (Figs. 5(*a*) and 5(*b*)) is found, but for larger Ra_S values. This phenomenon only exists in the oscillatory state.

4.2 Confined Layer. In a confined layer, only the set polynomial trial function (9) is used in the present study.

4.2.1 Change of Stability. A confined layer with an aspect ratio $A=1$ is considered here. Because of the computation time, calculations were done for only two f values (0.5 and 0.8) and for

Table 4 Values of stationary critical Rayleigh number determined by our method and by Giestas et al. studies as a function of solute Rayleigh number. With $A=1$, $Pr=7$, $Le=100$, $\mu_e=0.8$, and $f=0.5$.

Ra_S	Ra_T^{crit} Our Study[a]	Ra_T^{crit} Giestas[b]	Ra_T^{crit} Giestas[c]	Ra_T^{crit} Giestas[d]
100	9490	160	6045	3912
1000	90,433	1157	44,286	28,662
10,000	582,225	11,134	426,696	276,162
50,000	2,365,590	55,473	2,126,296	1,376,162

[a]Results from our study with truncation numbers $N=4$ and $M=5$.

[b]Results from Giestas et al. [13] considering the influence of solar radiation absorption.

[c]Results for Giastas et al. [14] with the influence of nonconstant diffusion coefficients.

[d]Results for Giastas et al. [14] study with the influence of both solar radiation absorption and non-constant diffusion coefficients.

the two μ_e values (0.2 and 0.8).

Table 3 shows results for $\mu_e=0.8$ and $f=0.5$. Variation of Ra_T^{crit} for different N and M values is minor for small values of Ra_S and is significant for larger values of Ra_S (reaching a maximum of 15%). Therefore, all figures in the steady state are shown for $N=2$ and $M=3$ because computations are much easier in this case and give similar precision than higher values of N and M.

From Tables 2 and 3, it is seen that convection starts much later than the infinite extension case. For small Ra_S values, critical Ra_T^{crit} values are multiplied by 1.5 and this rate increases as Ra_S increases.

One can see that convection is delayed when f or μ_e increases. Moreover, it can be seen from the bifurcation diagram in the (Ra_S, Ra_T) plan (Fig. 6) that the branches for the two f values are merely the same when $\mu_e=0.8$. However, when $\mu_e=0.2$, a large difference is predicted between the two branches; the difference increases when Ra_S increases. For small values of Ra_S (Fig. 6) the difference between the branches corresponding to the two f values are sensibly the same whatever the value of μ_e is.

4.2.2 Marginal Stability. In the oscillatory state, computations were perfomred for $(N=M=2)$ and $(N=M=3)$ for the case $\mu_e=0.8$ and $f=0.5$ (Table 3). It can be noted that there is a smaller difference between Ra_T^{over} for $N=M=2$ than for $N=M=3$. Henceforth, figures are given for $N=M=2$. Convection starts under the oscillatory state, whatever the Ra_S value is (Table 3).

Evolution of Ra_T^{over} as a function of Ra_S shows that for small Ra_S ($\leqslant 2000$) values, the behavior is similar to that observed in the steady state; convection is delayed for less transparent solutions and when f increases, with Ra_T^{over} close one to another. For Ra_S in the range (2000–4000), the phenomenon is inversed; convection is advanced when μ_e and f increase (Fig. 7(*a*)). The same behavior in the bifurcation diagram in the plan (Ra_S-ω) (Fig. 7) is predicted, but Ra_S values for which one observe this change in behavior is larger (10,000, 20,000) (Fig. 7(*b*)).

In our study, we considered only the influence of solar radiation absorption in the layer with constant diffusion coefficients and investigated the influence of truncation number on the convergence of the trial functions in order to minimize computation errors. Using the relation, given by Giestas et al. [14,15], between the stationary critical Rayleigh number and the problem parameters, we calculated the values of Ra_T^{crit} as a function of Ra_S for $f=0.5$, $\mu_e=0.8$, $q(d)=2.2$, $h_d=166.7$, $Pr=7$, $Le=100$, and for an aspect ratio $A=1$ (Table 4). The difference between our values of Ra^{crit} and those found by [14] is noticeable because the order of approximation used in their formulation is weak and does not allow one to get correct results. However, in such a formulation, considering nonconstant diffusivities, varying with temperature [15], improved their results, which are therefore concordant with our results (Table 4) obtained under the Boussinesq approximation (constant diffusivities).

5 Conclusion

Linear stability analysis was performed to study the stability of a plane layer with horizontal temperature and concentration stratification corresponding to the nonconvective zone of a solar pond. The cases of infinite layer with truncation number 5 and square layer with truncation number equal to 2 were investigated.

The study of the linear stability of the gradient zone of a solar pond of infinite and confined extension shows that the pure diffusive solution leads loose their stability via oscillatory solution in a solar pond. In the nonstationary case, for small values of Ra_S, the behavior is similar to that observed in the stationary case with the difference that convection starts later and for larger values of f. For larger value of Ra_S, the phenomenon is reversed, i.e., convection is stronger when μ_e and f increase. For an infinite fluid layer and for large values of Ra_S, our results are the same as those obtained by Veronis [11]; that is Ra_T^{over}/Ra_T^{crit} converges to 0.01.

Acknowledgment

This work has been supported by a CMCU (Comite Mixte de Cooperation Universitaire Franco-Tunisien) Project No. 00F1117.

Nomenclature

A = aspect ratio
C, c = concentration and perturbed concentration
d = depth of gradient zone, m
D = mass diffusivity, $m^2\ s^{-1}$
f = ratio of extracted heat flux to absorbed heat flux in the lower convective zone
g = acceleration of gravity, $m\ s^{-2}$
h_d = natural convection heat transfer coefficient, $W\ m^2\ K^{-1}$
Le = Lewis number
k^{ex} = exchange wave number
$\mathbf{r}$
$\mathbf{k}$ = unit vector pointing upward
N, M = truncature numbers
P = pressure
Pr = Prandtl number
$q(d)$ = heat flux at upper boundary ($z=d$), $W\ m^{-2}$
$\dot{q}$ = rate of energy generation
q_{tot} = total heat absorbed in the storage zone
q_{ext} = total heat extracted
Ra_S = Rayleigh numbers for salinity
Ra_T = Rayleigh number for temperature
Ra_T^{crit} = stationary critical Rayleigh
Ra_T^{over} = oscillatory critical Rayleigh
T = temperature
T_∞ = upper convective zone temperature
t = time, s
$\mathbf{V}$ = velocity field, $m\ s^{-1}$
u, w = velocity components, $m\ s^{-1}$

Symbols

α = coefficient of thermal expansion, K^{-1}
β = coefficient of salt expansion, K^{-1}
Ψ = stream function
ψ = perturbed stream function
λ = thermal conductivity of water, $W\ m^{-1}\ K^{-1}$
κ = thermal diffusivity, $m^2\ s^{-1}$
μ = dynamics viscosity, $m^2\ s^{-1}$
μ_e = extinction coefficient, m^{-1}
ρ, ρ_m = density and mean density, $kg\ m^{-3}$
θ = perturbation of temperature

ω = Hopf frequency

Subscripts

2 = upper surface
1 = down surface
s = steady state

References

[1] Weinberger, H., 1964, "The Physics of the Solar Pond," Sol. Energy, **8**(2), pp. 45–46.

[2] Tabor, H., 1981, "Solar Ponds," Sol. Energy, **27**, pp. 181–194.

[3] Rabl, A., and Nielsen, C. E., 1974, "Solar Ponds for Space Heating," Sol. Energy, **17**, pp. 1–12.

[4] Hull, J. R., Nielsen, C. E., and Golding, P., 1989, *Salinity-Gradient Solar Ponds*, CRC Press, Boca Raton.

[5] Hull, J. R., and Mehta, J. M., 1987, "Physical Model of Gradient Zone Erosion in Thermohaline Systems," Int. J. Heat Mass Transfer, **30**, pp. 1026–1036.

[6] Witte, J. M., 1989, "Thermal Brust Model of Double-Diffusive Interface," Ph.D. thesis, University at Urbana-Champaign.

[7] Hull, J. R., and Katti, Y., 1988, "Microconvection Effects at Double-Diffusive Gradient Zone Boundaries," Phys. Fluids, **31**, 2368–2370.

[8] Zangrando, F., and Fernando, H. J. S., 1991, "A Predictive Model for Migration of Double-Diffusive Interfaces," Sol. Energy, **113**, pp. 59–65.

[9] Sreenivas, K. R., Arakeri, J. H., and Srinivasan, J., 1995, "Modeling the Dynamics of the Mixed Layer in Solar Ponds," Sol. Energy, **54**(3), pp. 193–202.

[10] Veronis, G., 1965, "On Finite Amplitude Instability in Thermohaline Convection," J. Mar. Res., **23**, pp. 1–17.

[11] Veronis, G., 1968, "Effect of a Stabilizing Gradient of Solute on Thermal Convection," J. Fluid Mech., **34**, pp. 315–336.

[12] Schechter, R. S., Velarde, M. G., and Platten, J. K., 1974, "The Two-Component Bénard Problem," Adv. Chem. Phys., **26**, 265–301.

[13] Bemporad, G. A., and Rubin, H., 1994, "Analysis of the Instabilities Related to the Multiselective Injection and Withdrawal Procedures of the Advanced Solar Pond," Sol. Energy, **52**(6), pp. 533–539.

[14] Giestas, M., Pina, H., and Joyce, A., 1996, "The Influence of Radiation Absorption on Solar Pond Stability," Int. J. Heat Mass Transfer, **39**(18), pp. 3873–3885.

[15] Giestas, M., Pina, H., and Joyce, A., 1997, "The Influence of Nonconstant Diffusivities on Solar Ponds Stability," Int. J. Heat Mass Transfer, **40**(18), pp. 4379–4391.

[16] Karimi-Fard, M., Charrier-Mojtabi, M. C., and Mojtabi, A., 1999, "Onset of Stationary and Oscillatory Convection in a Tilted Porous Cavity Saturated With a Binary Fluid: Linear Stability Analysis," Phys. Fluids, **11**(6), pp. 1346–1358.

[17] Lanczos, C., 1938, "Trigonometric Interpolation of Empirical and Analytical Functions," J. Math. Phys., **17**, pp. 123–199.